

EXPANDED SEARCH FOR $Z \sim 10$ GALAXIES FROM HUDF09, ERS, AND CANDELS DATA: EVIDENCE FOR ACCELERATED EVOLUTION AT $Z > 8$?¹

P. A. OESCH^{2,†}, R. J. BOUWENS³, G. D. ILLINGWORTH², I. LABBÉ^{3,4}, M. TRENTI⁵, V. GONZALEZ², C. M. CAROLLO⁶, M. FRANK³, P. G. VAN DOKKUM⁷, D. MAGEE²

Draft version August 10, 2018

ABSTRACT

We search for $z \sim 10$ galaxies over ~ 160 arcmin² of WFC3/IR data in the Chandra Deep Field South, using the public HUDF09, ERS, and CANDELS surveys, that reach to 5σ depths ranging from 26.9 to 29.4 in H_{160} AB mag. $z \gtrsim 9.5$ galaxy candidates are identified via $J_{125} - H_{160} > 1.2$ colors and non-detections in any band blueward of J_{125} . Spitzer IRAC photometry is key for separating the genuine high- z candidates from intermediate redshift ($z \sim 2 - 4$) galaxies with evolved or heavily dust obscured stellar populations. After removing 16 sources of intermediate brightness ($H_{160} \sim 24 - 26$ mag) with strong IRAC detections, we only find one plausible $z \sim 10$ galaxy candidate in the whole data set, previously reported in Bouwens et al. (2011). The newer data cover a $3\times$ larger area and provide much stronger constraints on the evolution of the UV luminosity function (LF). If the evolution of the $z \sim 4 - 8$ LFs is extrapolated to $z \sim 10$, six $z \sim 10$ galaxies are expected in our data. The detection of only one source suggests that the UV LF evolves at an accelerated rate before $z \sim 8$. The luminosity density is found to increase by more than an order of magnitude in only 170 Myr from $z \sim 10$ to $z \sim 8$. This increase is $\geq 4\times$ larger than expected from the lower redshift extrapolation of the UV LF. We are thus likely witnessing the first rapid build-up of galaxies in the heart of cosmic reionization. Future deep HST WFC3/IR data, reaching to well beyond 29 mag, can enable a more robust quantification of the accelerated evolution around $z \sim 10$.

Subject headings: galaxies: evolution — galaxies: high-redshift — galaxies: luminosity function

1. INTRODUCTION

In recent years, great progress has been made in quantifying the evolution of the galaxy population at the end of cosmic reionization around $z \sim 6$. Deep Hubble Space Telescope (HST) legacy fields, such as the Hubble Ultra-Deep Field (HUDF; Beckwith et al. 2006) or GOODS (Giavalisco et al. 2004), and wide area ground-based imaging, have made it possible to study the evolution of the UV luminosity function (LF) across $z \sim 4 - 6$ to great accuracy (e.g. Bouwens et al. 2007; Oesch et al. 2007; Iwata et al. 2007; Ouchi et al. 2004; Sawicki & Thompson 2006; McLure et al. 2009).

Over the last two years, with the installation of the Wide Field Camera 3 (WFC3) onboard the HST, the observational frontier of galaxies has now been pushed into the reionization epoch, as deep WFC3/IR data led to the identification of more than 100 galaxy candidates at $z \sim 6.5 - 8.5$ (e.g. Bouwens et al. 2011b; Bouwens et al. 2010a; Oesch et al. 2010c; McLure et al. 2010; Bunker et al. 2010; Finkelstein et al. 2010; Yan et al. 2010; Wilkins et al. 2010, 2011a;

Lorenzoni et al. 2011; Trenti et al. 2011). This is essential for estimating the contribution of galaxies to cosmic reionization. One of the most important conclusions from these studies is thus the realization that the UV luminosity density (LD) emitted by the galaxy population gradually falls towards higher redshifts. For example, the LD of the $z \sim 3$ galaxy population is about an order of magnitude larger than that of the $z \sim 8$ population, about 1.5 Gyr earlier.

How this evolves to even higher redshifts is still very unclear. A sizable galaxy population at $z \gtrsim 9$ is expected based on the first estimates of stellar population ages of $z \sim 7 - 8$ galaxies, indicating that these sources very likely started forming stars already at $z \gtrsim 10 - 12$ (e.g. Labbé et al. 2010b,a; Finkelstein et al. 2010; Gonzalez et al. 2010). This is still somewhat uncertain due to possible nebular line emission contaminating the Spitzer photometry (e.g. Schaerer & de Barros 2010). Nonetheless, an early epoch of star-formation is also required by the mean redshift of reionization as measured by WMAP ($z_r = 10.6 \pm 1.2$; Komatsu et al. 2011), if galaxies are assumed to be the main drivers for this process.

However, previous searches for $z \gtrsim 9$ sources in the pre-WFC3 era only resulted in very small samples of relatively low reliability candidates, none of which have been confirmed (e.g. Bouwens et al. 2005; Stark et al. 2007; Henry et al. 2008, 2009; Richard et al. 2008). This is mainly due to the extreme faintness of the $z \sim 10$ galaxy population. Not only are these galaxies fainter due to their increased distance, but also they are expected at intrinsically lower luminosities. Additionally, the detection of such high-redshift sources is further complicated

¹ Based on data obtained with the *Hubble Space Telescope* operated by AURA, Inc. for NASA under contract NAS5-26555.

² UCO/Lick Observatory, University of California, Santa Cruz, CA 95064; poesch@ucolick.org

[†] Hubble Fellow

³ Leiden Observatory, Leiden University, NL-2300 RA Leiden, Netherlands

⁴ Carnegie Observatories, Pasadena, CA 91101

⁵ University of Colorado, Center for Astrophysics and Space Astronomy, 389-UCB, Boulder, CO 80309, USA

⁶ Institute for Astronomy, ETH Zurich, 8092 Zurich, Switzerland

⁷ Department of Astronomy, Yale University, New Haven, CT 06520

by the fact that they are invisible in optical data. Due to the highly neutral inter-galactic medium before the end of cosmic reionization, their UV photons are absorbed shortward of the redshifted Ly α line, which shifts to $> 1\mu\text{m}$ at $z \gtrsim 7$. Thus, these sources can only be seen in the NIR, where previous detectors were significantly lagging behind optical technology.

With $40\times$ higher efficiency relative to NICMOS to detect high redshift galaxies in the NIR, WFC3/IR has the potential to change this and to push galaxy studies to beyond $z \sim 9$. Several deep and wide area WFC3/IR data sets have been taken already and several more are upcoming. The challenge for identifying genuine $z > 9$ sources in these data sets, is that these galaxies will only be visible in one band (H_{160}). This has already led to some controversy in the first searches for $z \sim 10$ sources in the first-epoch WFC3/IR data over the Hubble Ultra Deep Field (see e.g. Bouwens et al. 2011a; Yan et al. 2010). In our recent analysis, which includes the full two-year WFC3/IR data over the HUDF as well as the shallower, but wider Early Release Science (ERS) data, Bouwens et al. (2011a) found only one single galaxy candidate detected at $> 5\sigma$ with an estimated redshift at $z \sim 10.3$. Given that about three should have been detected, if the evolution of the LF continued as extrapolated from the trends established across $z \sim 4$ to $z \sim 6$, this provided first tentative evidence for an accelerated evolution in the galaxy population from $z \sim 8$ to $z \sim 10$.

In this paper we significantly expand on our first $z \sim 10$ analysis from WFC3/IR data presented in Bouwens et al. (2011a) by extending the search to all the deep WFC3/IR fields in the Chandra Deep-Field South area that have since become available. The inclusion of the two deep HUDF09 parallel fields is especially useful, since both reach just ~ 0.5 mag shallower than the ultra-deep HUDF field but triple the search area for $\sim 28 - 29$ AB mag sources. Additionally, we use different analysis tools developed by the first author that provide an independent analysis of the HUDF and ERS data. While the Lyman-Break approach is similar in principle to that of Bouwens et al. (2011a) the use of independently tested software and procedures for the source detection and its analysis provides confirmation and validation. The expanded data set also covers $> 3\times$ the area at moderately deep ~ 26.5 AB mag, thanks to the inclusion of the first epochs of CANDELS data over these fields. This will be used to constrain the evolution of the galaxy population over the ~ 200 Myr from $z \sim 10$ when the universe was ~ 500 Myr old to $z \sim 8$ at ~ 700 Myr.

We start by describing the full data set in §2 and present the $z \sim 10$ candidate selection and its efficiency in §3. In §4 we present our new constraints on the LF at $z \sim 10$. We will refer to the HST filters F435W, F606W, F775W, F850LP, F098M, F105W, F125W, F160W as B_{435} , V_{606} , i_{775} , z_{850} , Y_{098} , Y_{105} , J_{125} , H_{160} , respectively. Throughout this paper, we adopt $\Omega_M = 0.3$, $\Omega_\Lambda = 0.7$, $H_0 = 70 \text{ km s}^{-1} \text{ Mpc}^{-1}$, i.e. $h = 0.7$. Magnitudes are given in the AB system (Oke & Gunn 1983).

2. THE DATA

Our analysis is based on the public WFC3/IR data sets that are available over the GOODS South fields (Giavalisco et al. 2004) as a result of three different pro-

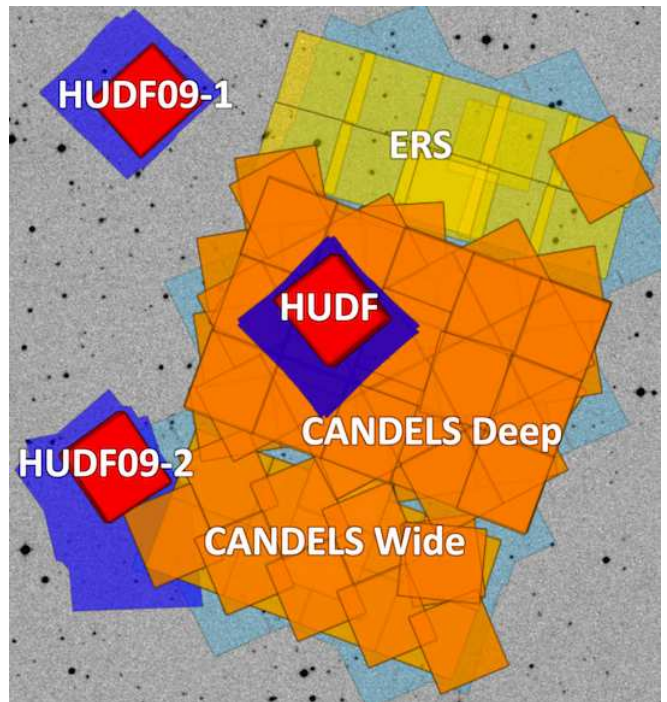


FIG. 1.— The WFC3/IR fields (orange) around the GOODS South area used in this analysis (see §2 and Table 1). The HUDF/HUDF09-1/HUDF09-2 fields comprise the deepest NIR data available to date, reaching to $\gtrsim 29$ AB mag. These three WFC3/IR pointings are covered in a total of 192 HST orbits, which obtained photometry in Y_{105} , J_{125} , and H_{160} . The ERS field consists of 60 orbits of WFC3/IR imaging in Y_{098} , J_{125} , and H_{160} spread over a 2×5 tile. The CANDELS program is an on-going multi-cycle treasury survey consisting of two parts: CANDELS-Deep ($\sim 60 \text{ arcmin}^2$, limited at $H_{160,AB} \sim 27.5$) and CANDELS-Wide ($\sim 40 \text{ arcmin}^2$, limited at $H_{160,AB} \sim 26.9$). Only J_{125} and H_{160} data obtained before August 6, 2011 is used in this analysis (together with the shallow Y_{105} imaging of CANDELS Wide).

grams (HUDF09, ERS, and CANDELS), which we describe below. The outline of all fields is shown in Figure 1. The key feature of these fields is that they have WFC3/IR coverage in J_{125} and H_{160} , which will be used to select $z \sim 10$ sources. Additionally, they have deep optical coverage as well as deep IRAC imaging, which is essential to exclude low redshift contamination (see section 3).

All the WFC3/IR data has been reduced following standard procedures outlined, e.g., in Bouwens et al. (2011b). In particular, our reduction pipeline includes the subtraction of a super median image, careful image registration to the ACS frames and an automatic elimination of pixels affected by persistence. The final pixel scale of the images in our analysis is set to $0''.06$. A summary of the HST data used in this analysis can be found in Table 1. The final resolution of the WFC3/IR data is $\sim 0''.16$ (FWHM), and $\sim 0''.09$ in the optical ACS data.

The ACS data on the GOODS fields we used are the v2 reductions that are publicly available from MAST⁹ (M. Giavalisco and the GOODS Team, in preparation). The Spitzer data are the GOODS IRAC images (Dickinson et al. 2003) as made publicly available by the SIMPLE team (see e.g. Damen et al. 2009). Additionally, we include the newly acquired Spitzer IRAC [3.6

⁹ <http://archive.stsci.edu/prepds/goods/>

TABLE 1
SUMMARY OF 5σ DEPTHS^a OF OBSERVATIONAL DATA USED IN OUR ANALYSIS

Field	Area [arcmin ²]	B_{435}	V_{606}	i_{775}	z_{850}	$Y_{098/105}$	J_{125}	H_{160}
HUDF09	4.7	29.2	29.6	29.4	28.8	29.1	29.3	29.4
HUDF09-1 ^b	4.7	—	28.9	28.7	28.6	28.6	28.8	28.6
HUDF09-2 ^b	4.7	28.8	29.3	28.9	28.7	28.6	28.9	28.9
ERS	41.3	27.8	28.0	27.5	27.2	27.4	27.8	27.6
CANDELS-Deep ^b	63.1	27.8	28.0	27.5	27.2	—	27.7	27.5
CANDELS-Wide ^b	41.9	27.8	28.0	27.5	27.2	27.1	27.2	26.9

^a Measured in circular apertures of $0''.25$ radius.

^b New relative to Bouwens et al. (2011a) for $z \sim 10$ search.

and [4.5] data over the HUDF field from the IUDF10 survey (proposal 70145, PI: Labbé). This so far adds ~ 130 h of observations, which increases the depth in both filters by an additional ~ 0.4 mag. Where available, we also matched our WFC3/IR sources with the publicly available GOODS-MUSIC multi-band photometry catalog of Santini et al. (2009).

2.1. Full HUDF09 Data Set

The HUDF09 program (PI: Illingworth; Bouwens et al. 2011b) consists of 192 HST orbits to provide ultra-deep WFC3/IR imaging over three pointings centered on the HUDF (Beckwith et al. 2006) and its two parallel fields from the UDF05 program (PI: Stiavelli; Oesch et al. 2007). The program has been completed, providing the deepest IR images ever taken. It comprises 3×4.7 arcmin² imaging in the three filters Y_{105} , J_{125} , and H_{160} , reaching down to $H_{160,AB} = 29.4, 28.6$, and 28.9 (5σ in $0''.5$ diameter apertures) for the HUDF, HUDF09-1, and HUDF09-2, respectively (see Fig. 1). For a more detailed description of this data set and the data reduction see Bouwens et al. (2011b).

2.2. Wide Area Data

In addition to the ultra-deep HUDF09 data, we also analyzed shallower, wider area WFC3/IR imaging from the ERS and CANDELS programs, in order to constrain the volume density of more luminous star-forming galaxies at $z \sim 10$.

The Early Release Science Data (ERS) provide WFC3/IR imaging of ~ 41 arcmin² of the northern part of the GOODS South field. Two orbits of WFC3/IR imaging were obtained in each of the filters Y_{098} , J_{125} , and H_{160} , over a 2×5 grid of pointings (60 orbits in total). These data are reduced in an analogous way to our HUDF09 data, and are aligned and drizzled to the GOODS ACS mosaics after rebinning to a $0''.06$ pixel scale. These data reach to $H_{160} = 27.6$ (see also Bouwens et al. 2011b). For a more detailed description of this data set see Windhorst et al. (2011).

The last two fields included in our analysis are obtained as part of the Multi-Cycle Treasury program CANDELS (PI: Faber/Ferguson; Grogin et al. 2011; Koekemoer et al. 2011). In particular, we include the first six visits of the CANDELS-Deep program (obtained until August 6, 2011), which covers the central part of GOODS South in 3×5 tiles with ~ 6000 s exposures in both J_{125} and H_{160} in a total of 92 orbits. This data covers ~ 63 arcmin² and reaches to $H_{160,AB} \sim 27.5$ mag. Additionally, we also included the imaging data

of the supernova follow-up program of CANDELS (PI: Riess), which adds imaging over two pointings over CANDELS Deep (one of which is essentially centered on the HUDF). Finally, we made use of the 29 orbits of WFC3/IR data of the CANDELS-Wide survey (Y_{105} , J_{125} and H_{160} , obtained until March 29, 2011). These comprise 9 WFC3/IR pointings (~ 42 arcmin²), completing the coverage of the GOODS South field, and reach to $H_{160,AB} = 26.9$ (~ 2000 s exposures). As for the ERS, the WFC3/IR data of the CANDELS program has been aligned to the GOODS ACS mosaics with a pixel scale of $0''.06$. The part of the CANDELS field overlapping with the WFC3/IR HUDF has been omitted when analyzing this data set in order not to duplicate the analysis of that area.

We will subsequently refer to the combination of the ERS and the two CANDELS fields as ‘Wide Fields’.

3. SOURCE SELECTION

3.1. Catalog Construction

Source catalogs are derived with the SExtractor program (Bertin & Arnouts 1996), which is used to detect galaxies in the H_{160} images and perform matched aperture photometry on PSF-matched images. The colors used here are based on isophotal apertures derived from the H_{160} images, and total magnitudes are measured in standard 2.5 Kron apertures, corrected by 0.2 mag in order to account for flux loss in the PSF wings.

The detection significance of sources was established in $0''.25$ radius apertures. The RMS maps were scaled based on the detected variance in 1000 random apertures for each WFC3/IR frame on empty sky regions after 3σ clipping. This procedure ensures that the SExtractor weight maps correctly reproduce the actual noise in the images. Subsequently only sources with signal-to-noise ratios larger than 5 (in $0''.25$ radius apertures) in H_{160} are considered.

3.2. J_{125} -dropout Candidate Selection

Galaxies at $z > 9.5$ are expected to exhibit very red $J_{125} - H_{160}$ colors since the redshifted, strong Ly α absorption (by the predominantly neutral inter-galactic hydrogen) cuts into the flux in the J_{125} filter (see Figure 2). This makes such high redshift galaxies completely invisible blueward of J_{125} , and we use this fact for their identification.

As can be seen from Figure 2, however, also passively evolving or dusty galaxies at intermediate redshifts ($z \sim 2.5 - 4$) can exhibit similarly red colors in $J_{125} - H_{160}$. While the requirement of optical non-detections removes

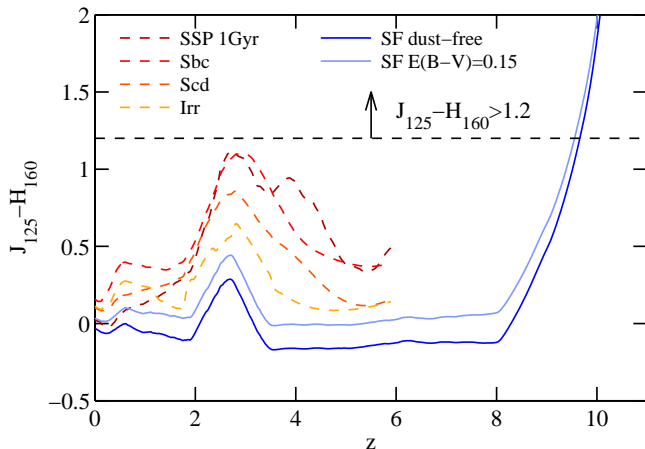


FIG. 2.— Color selection of $z > 9.5$ galaxies (§3.2). Shown are the $J_{125} - H_{160}$ colors of different types of galaxies as a function of their redshift. Star-forming galaxies are shown as solid blue lines. The lighter blue spectral energy distribution (SED) is reddened by $E(B-V) = 0.15$ mag using a Calzetti et al. (2000) dust law. As the Ly α absorption due to intergalactic neutral hydrogen shifts into the J_{125} band, galaxies start to exhibit progressively redder colors beyond $z \sim 8$. A selection with $J_{125} - H_{160} > 1.2$ thus identifies galaxies at $z \gtrsim 9.5$. Strong Balmer and 4000 Å breaks in evolved $z \sim 3$ galaxies, combined with some dust obscuration can also result in very red $J_{125} - H_{160}$ colors. The dashed lines correspond to more evolved galaxies dominated by progressively older stellar populations from the library of Coleman et al. (1980) as well as a 1 Gyr old single stellar population (SSP) from the library of Bruzual & Charlot (2003). Spitzer IRAC data provides a way to separate these different populations at intermediate and very high redshifts (see text and Fig. 3).

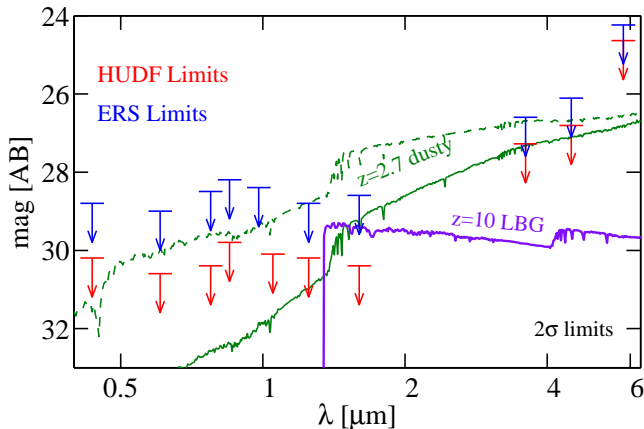


FIG. 3.— Sensitivity limits (2σ) of the data used in this analysis. The red arrows indicate the limits of the ACS, WFC3/IR and IRAC data over HUDF, while blue arrows correspond to the ERS data set. The SED of a $z = 10$ star-forming galaxy is plotted in purple, showing the distinguishing feature of complete absorption shortward of the redshifted Ly α line. Evolved and dusty galaxy SEDs can mimic the same features as a $z \sim 10$ source, i.e. red $J_{125} - H_{160}$ and undetected in the optical data, unless this is extremely deep. Such sources are typically detected in the IRAC data. Alternatively, the solid and dashed green lines show possible SEDs of $z \sim 2.7$ galaxies which could escape the IRAC detection at 2σ . These correspond to evolved galaxies (500 Myr), with moderate amounts of dust extinction, and are normalized to the 5σ detection limits of the H_{160} bands. Note that much larger amounts of dust can be hidden for interloper galaxies at the detection limit of the HUDF (green solid, $A_V = 2.0$ mag) than for the ERS (green dashed, $A_V = 0.6$ mag). Thus even with IRAC it can be a challenge to separate real $z \sim 9 - 10$ sources from lower redshift contaminants.

the bulk of lower redshift contamination, certain intermediate redshift galaxies with evolved or dusty stellar populations can still be included due to the fact that the optical data does not reach deep enough, if at similar depth as the IR (see Fig. 3). Deep Spitzer IRAC data provides a way to identify contaminating galaxies. These are expected to exhibit very red $H_{160} - [3.6\mu\text{m}]$ colors, which discriminates them from genuine $z \sim 10$ candidates.

To exclude possible low-redshift contamination, we thus use two steps to select $z \gtrsim 9.5$ galaxy candidates. For the first step, the primary criteria are based on HST data only:

$$(J_{125} - H_{160}) > 1.2$$

$$S/N(H_{160}) > 5 \quad \wedge \quad S/N(< J_{125}) < 2 \quad \wedge \quad \chi_{opt}^2 < \chi_{cut}^2$$

Additional to excluding objects that are detected in any band blueward of J_{125} at more than 2σ , we include a cut in the optical χ_{opt}^2 value of a galaxy (see e.g. Bouwens et al. 2011b; Bouwens et al. 2011a). This is computed from the $0''.25$ radius aperture fluxes as $\chi_{opt}^2 = \sum_i \text{sign}(f_i) (f_i/\sigma_i)^2$, where the sum runs over all the bands available in the given data set blueward of J_{125} , i.e. it includes all the available optical data as well as the NIR band Y_{105} for the HUDF09 data, and Y_{098} in the ERS. The relatively large apertures were chosen in order sample $> 70\%$ of the light of point-like sources.

The limiting χ_{cut}^2 are derived from photometric scatter simulations. They are set to exclude the majority of interlopers which remain undetected at 2σ purely due to photometric noise, but not to cut a substantial fraction of galaxies with real zero flux in the optical bands. The scatter simulations utilize all galaxies in our catalogs that are 1 – 3 mag above the completeness limit, applying photometric Gaussian noise from 1 mag fainter sources. From these simulations it is clear that contamination is mainly an issue at 0.75 mag above the completeness limits, but that $\sim 60 - 80\%$ of contaminants can be eliminated by using a χ_{opt}^2 limit of $\chi_{cut}^2 = 2.8$ or 2.4, for 5 filters or 4 filters, respectively. In the HUDF09 data, the resulting number of expected contaminants due to photometric scatter is thus reduced from ~ 0.5 source per WFC3/IR field to ~ 0.1 source.

On the other hand, the adopted χ_{cut}^2 limits do remove an additional $\sim 20\%$ of sources with real zero flux, simply due to Gaussian statistics. This reduction of the real galaxy sample is reflected in our subsequent analysis in the reduction of the selection volume.

All galaxies passing the above selection criteria, using both the ACS and WFC3/IR data, are retained and analyzed individually. These total to 17 sources with $H_{160,AB}$ in the range 23.6 – 28.8 mag; one source in the HUDF, none in the parallel HUDF09 fields, three in the ERS and 8 and 5 in the CANDELS Deep and Wide, respectively (see Tables 2 and 4).

Interestingly, only one source (the previously reported galaxy with $H_{160} \sim 29$ mag from Bouwens et al. 2011) did pass our selection in the three deep HUDF09 fields, while the shallower CANDELS and ERS fields contribute a total of 16 sources (all with $H_{160,AB} \lesssim 26$ mag). Upon inspection of their images, it turns out that all these brighter sources are very well detected in the IRAC data, even in the shallow $8.0\mu\text{m}$ band. Their measured

TABLE 2
THE $z \sim 10$ GALAXY CANDIDATE

ID	α	δ	H_{160}	$J_{125} - H_{160}$	$S/N_{H_{160}}$
HUDFj-39546284	03:32:39.54	-27:46:28.4	28.8 ± 0.2	> 2.02	6.3

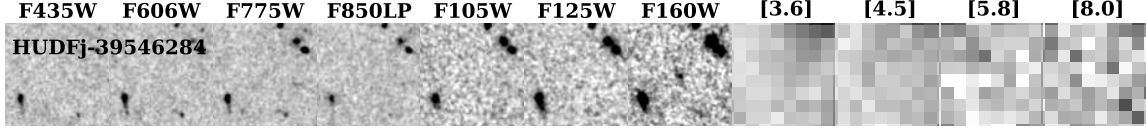


FIG. 4.— $5'' \times 5''$ images of our only viable $z \sim 10$ galaxy candidate (see also Bouwens et al. 2011a). The images show, from left to right, B_{435} , V_{606} , i_{775} , z_{850} , Y_{105} , J_{125} , H_{160} , IRAC [3.6], [4.5], [5.8], and [8.0]. The J_{125} and H_{160} images shown here are combined from both the HUDF09 and the CANDELS survey data (which add 0.05 mag in depth). The IRAC [3.6] and [4.5] images include the additional ~ 130 h of data obtained over the HUDF as part of the IUDF10 program so far. As can be seen, the source is only significantly detected in H_{160} . The IRAC $[3.6\mu\text{m}]$ data shows a non-negligible excess of flux in the vicinity of the candidate. However, this flux is very likely to be associated with the brighter neighboring source to the upper right. After subtraction of all nearby sources in IRAC, the candidate is undetected in both IRAC bands at less than 1σ . The images are oriented N top, E left.

$H_{160} - [3.6]$ colors are in the range $1.6 - 4.3$, which, for a $z \sim 10$ source, would correspond to a UV continuum slope $\beta \gtrsim -0.2$, or a dust reddening with $A_V > 1.6$ mag. Given that galaxies at the bright end of the $z \sim 7$ population are measured to have very low extinction values and continuum slopes of $\beta \simeq -2.0 \pm 0.2$ (see e.g. Bouwens et al. 2010b; Finkelstein et al. 2010; Dunlop et al. 2011; Wilkins et al. 2011b), the extremely red colors of these galaxies rules out $z \gtrsim 9$ solutions with any sensible SED.

All sources with IRAC detections are thus removed from our sample of potential $z \sim 10$ galaxies, reducing the sample to one single candidate in the HUDF, previously reported in Bouwens et al. (2011a, see Figure 4 and Table 2). The 16 removed sources are shown in the appendix in Figure 11 and listed in Table 4.

3.3. The $z \sim 10$ Galaxy Candidate

Images of the only possible $z \sim 10$ galaxy candidate are shown in Figure 4. The source is detected at 6.3σ in H_{160} (measured in circular apertures of $0''.25$ radius). This is higher but completely consistent with the Bouwens et al. (2011a) significance estimates, which are based on smaller apertures. As can be seen, the source is not significantly detected in any other band. Its value of $\chi^2_{opt} = 2.77$ is very close, but just below the limit of $\chi^2_{cut} = 2.8$. This is mainly due to a 1.5σ flux excess in i_{775} , which appears to be due to an extended structure in the background of that image. When adopting smaller apertures, the χ^2_{opt} value is found to be reduced, indicating also that this excess of flux is not associated with the source itself.

The Spitzer IRAC $3.6\mu\text{m}$ data shows some flux from a nearby source. However, after subtraction of all the neighboring sources in IRAC, the candidate is undetected (0.09σ), with a 2σ upper limit on its IRAC [3.6] magnitude of > 27.2 mag AB (Gonzalez et al., in prep.). This thus corresponds to $H_{160} - [3.6] < 1.6$ at 2σ , which is much bluer (by > 0.4 mag) than the typical low-redshift contaminants that we culled from our sample (see also next section). After adding the newly acquired IRAC data from the IUDF10 program (Spitzer proposal 70145, PI: Labbe) to the GOODS IRAC data and removing neighboring sources, the $z \sim 10$ candidate is also un-

detected at [4.5] ($S/N = 0.3$) providing added weight to the likelihood of it being at high rather than low redshift.

We derive the photometric redshift of the candidate using the code ZEBRA (Feldmann et al. 2006; Oesch et al. 2010b) with synthetic stellar population models from Bruzual & Charlot (2003) to which we added nebular continuum and line emission following, e.g., Schaerer & de Barros (2009). Using the full 11 band fluxes and flux errors, we derive a photometric redshift for this source of $z_{phot} = 10.4^{+0.5}_{-0.4}$, with a likelihood of a low redshift solution at $z < 8$ of $< 6\%$. The full spectral energy distribution (SED) of the source and its redshift likelihood function are shown in Figure 5. The best-fit SED corresponds to a very young, dust-free star-burst (see also Gonzalez et al. in prep.).

The best low redshift solution is found at $z_{lowz} = 2.7$, for an evolved, very low mass galaxy SED ($M = 3 \times 10^8 M_\odot$) with moderate extinction. Interestingly, this SED is expected to be detected only at $\sim 1.5\sigma$ in J_{125} , but it nevertheless has a significantly higher χ^2 value (13.7 compared to $\chi^2_{best} = 7.0$). Deeper HST data shortward of the break would be extremely useful in order to constrain the possible non-detection of the source shortward of $1.4\mu\text{m}$. As with other high-redshift catalogs, the added shorter-wavelength optical/near-IR data would play a key role in helping to further tighten its photometric redshift measurement.

3.4. The Dusty and Evolved Contaminants of J_{125} -Dropout Selections

The properties of the 16 intermediate brightness sources that did not pass the IRAC non-detection criteria are discussed in the appendix. From fitting their SEDs, these sources are found to be mostly massive galaxies ($M > 5 \times 10^{10} M_\odot$) with obscured but evolved stellar populations at $z \sim 2 - 4$.

Interestingly, all these galaxies are essentially limited to $H_{160} \sim 24 - 26$ mag. This is ~ 1 mag brighter than the detection limits of our bright survey fields (see Figure 10 in the appendix), and thus suggests that such very red galaxies have a somewhat peaked luminosity function. This will have to be confirmed and quantified with future wide area data. However, at face value, it would appear that contamination from such sources with $J_{125} - H_{160} >$

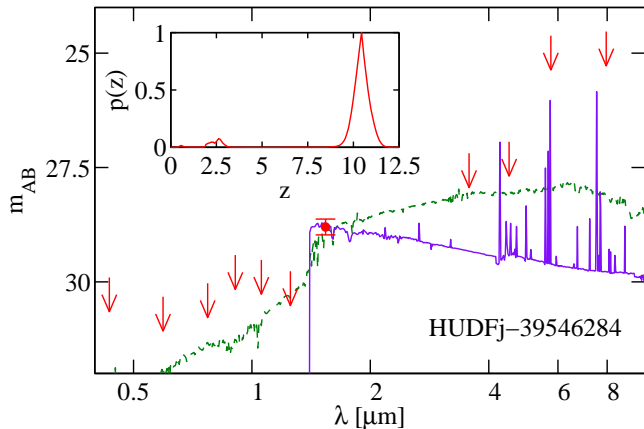


FIG. 5.— Best-fit SED of the only viable $z \sim 10$ candidate, previously reported in Bouwens et al. (2011a). The measured photometry is shown with the red circle with errorbars and with 2σ upper limits in case of non-detections. All fluxes and flux errors were used in the SED fit, however, even if they were negative. The best fit SED is found at $z_{phot} = 10.4$ and is shown as a solid line ($\chi^2_{best} = 7.0$), corresponding to a dust-free, young galaxy. The best template for a low redshift solution is also shown as the dashed green line. This SED has a redshift of $z_{lowz} = 2.7$, and is passive with an age of 650 Myr and of rather low mass (only $3 \times 10^8 M_\odot$). Additionally, the low- z SED is reddened with $E(B-V) = 0.1$ mag. Based on its larger χ^2 value ($\chi^2_{lowz} = 13.7$), this SED is formally excluded at $> 90\%$ probability, however. The redshift probability function is shown in the inset in the upper left. The sharp decrease above $z \sim 10.5$ of $p(z)$ is due to the use of a LF prior at $z > 8$ and due to the fact that Ly α absorption starts affecting the H_{160} band (which would require the source to be brighter intrinsically).

1.2, and with $H_{160} - [3.6] \gtrsim 2$ is less problematic at fainter magnitudes. We note, however, that contamination from similar galaxies with less extreme colors (which may be more abundant also at $H_{160} > 26$ mag) may still be non-negligible due to photometric scatter (see also §3.5).

Furthermore, it is interesting to note that it is very difficult to construct clean $z \sim 10$ galaxy samples purely based on HST data alone. Even if we were to increase the color criteria to $J_{125} - H_{160} > 2.0$, there would still be two contaminating galaxies in the sample together with our only viable $z \sim 10$ candidate. Thus, also for future constraints on the bright end of the $z \sim 10$ LF, it will be important to perform additional follow-up studies to validate the candidates, e.g. with Spitzer. This will be less of a concern for future $z \sim 9$ galaxy samples, which can be obtained, e.g., based on new F140W filter data. In such a data set intrinsically red galaxies can be sorted out by requiring a blue continuum across F140W and H_{160} .

3.5. Possible Sources of Sample Contamination

Here, we only give a brief summary of the possible sample contamination. For a thorough discussion we refer the reader to Bouwens et al. (2011a).

Essentially, the only probable chance for contamination is due to photometric scatter of a red lower redshift source. We estimate this to be a 10% chance based on our photometric scatter experiments described in section 3.2, including the χ^2_{opt} cuts.

Other typical contaminants to LBG selections such as very cool dwarf stars and supernovae can essentially be excluded based on the relatively blue $J_{125} - H_{160}$ (< 1.1) colors of stellar SEDs, on the fact that the source

is detected in both the first and the second year of the HUDF09 WFC3/IR data, and due to the fact that the candidate shows clear signs of an extended morphology.

Additionally, it is very unlikely that this source is spurious, since the flux distribution in circular apertures randomly distributed over empty regions of the HUDF H_{160} image are nearly exactly Gaussian, and the source is well detected at 6.3σ .

4. THE ABUNDANCE OF $Z \sim 10$ GALAXIES

In this section we compute the expected abundance of $z \sim 10$ galaxies in our dataset, and derive constraints on the $z \sim 10$ LF based on our data.

4.1. Completeness and Selection Functions

In order to estimate the number of sources we expect in our data from a given LF, we have to estimate the completeness as a function of magnitude $C(m)$ and selection function as a function of redshift and magnitude $S(z, m)$. Following Oesch et al. (2007, 2009), this is done by inserting artificial galaxies in the observational data and rerunning the source detection with the exact same setup as for the original catalogs. This is done for each of our fields individually.

Two sets of simulations were run. In the first set, we follow Bouwens et al. (2003), where the artificial galaxies are ‘cloned’ from the $z \sim 4$ dropout sample of the GOODS and HUDF fields. The images of these sources are adjusted for surface brightness dimming, the difference in angular diameter distance, as well as a size scaling of $(1+z)^{-1}$ as observed for the Lyman Break galaxy population across $z \sim 3 - 7$ (see e.g. Ferguson et al. 2004; Bouwens et al. 2004; Oesch et al. 2010a). These are then inserted in the observed images with galaxy colors as expected for star-forming galaxies between $z = 8$ and $z = 12$. When computing the galaxy colors we assume a distribution of UV continuum slopes with $\beta = -2.5 \pm 0.4$ (see e.g. Bouwens et al. 2009, 2010b; Finkelstein et al. 2010; Stanway et al. 2005).

From these simulations, we compute the completeness as a function of observed $H_{160,AB}$ magnitude for each field, taking into account the scatter and offsets between input and output magnitudes. Additionally, we compute the selection probabilities as a function of redshift and magnitude by measuring the fraction of sources that meet our selection criteria. By construction, galaxies are selected at $> 50\%$ at redshifts $z \gtrsim 9.5$.

In the second set of simulations, we repeat the above procedure. However, instead of using observed galaxy images, we use theoretical galaxy profiles from a mix of exponential (Sersic $n = 1$) and de Vaucouleur (Sersic $n = 4$) profiles. The size distribution is chosen to be log-normal, again with the same size scaling as a function of redshift. The completeness and selection functions of our two procedures are in excellent agreement. This demonstrates the reliability of our approach, which appears to be essentially independent of the adopted galaxy profiles (unlike what has been claimed elsewhere, e.g. Grazian et al. 2010, but see also Bouwens et al. 2010b).

4.2. The Expected Number of $z \sim 10$ Sources

The expected number of sources in a given magnitude bin m_i can be estimated for any given LF, $\phi(M)$,

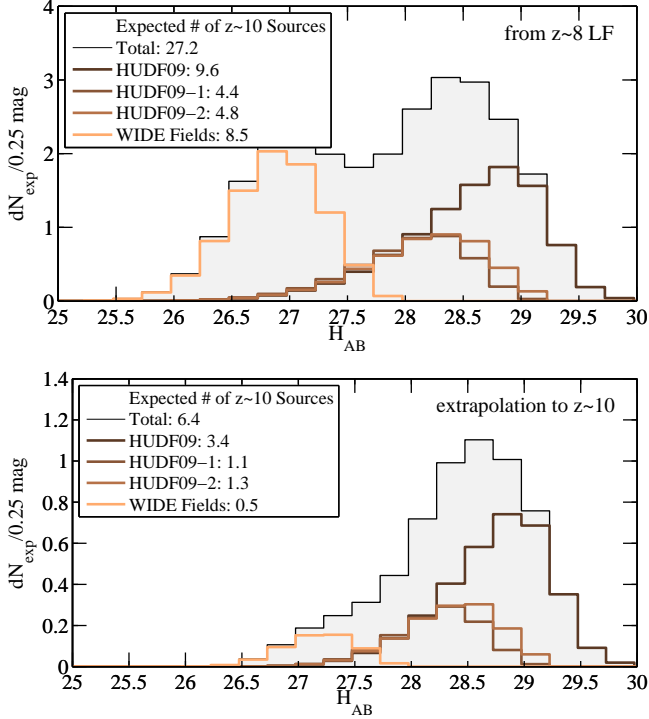


FIG. 6.— Expected number of $z \sim 10$ candidates in the different fields assuming the LF to be as measured at $z \sim 8$ (top; Bouwens et al. 2011b) or as expected from extrapolating the $z \sim 4 - 8$ trends to $z \sim 10$ (bottom). The one detected source is in stark contrast to the ~ 27 sources expected if the LF was constant across the 170 Myr from $z \sim 10$ to $z \sim 8$. The LF appears to evolve at a significantly accelerated pace with respect to the empirical evolution observed across $z \sim 4 - 8$. 6 sources at $z \sim 10$ should be detected when extrapolating the lower redshift trends, while only one probable candidate is found.

through:

$$N_i^{\text{exp}} = \int_{\Delta m} dm \int dz \frac{dV}{dz} S(m, z) C(m) \phi(M[m, z])$$

The result of this calculation is shown in Figure 6 for each individual field using the observed LFs at $z \sim 8$ (Bouwens et al. 2011b), as well as that expected at $z \sim 10$. The latter is based on extrapolating the evolution of the Schechter function parameters presented in Bouwens et al. (2011b), which is based on fitting the likelihood contours of LBG LFs across $z \sim 4 - 8$. In particular, significant evolution is only seen in the characteristic luminosity M_* , which is found to dim by 0.33 mag per unit redshift. The other two Schechter function parameters were kept constant, in agreement with the small evolutionary trends that were found at low significance in Bouwens et al. (2011b). For reference, the final parameter evolution we use in this work is:

$$M_*(z) = -21.02 \text{ mag} + (z - 3.8) \times 0.33 \text{ mag}$$

$$\phi_* = 1.14 \times 10^{-3} \text{ Mpc}^{-3} \text{ mag}^{-1} = \text{const}$$

$$\alpha = -1.73 = \text{const}$$

As can be seen in Figure 6, the wide-area, shallow data of CANDELS and ERS are very useful for constraining the evolution in the bright end of the LF. In particular, if there was no evolution in the LF from $z \sim 10$ to $z \sim 8$,

the wide area data should contain 8.5 $z \sim 10$ sources. In total, we would expect to see ~ 27 sources if the LF was unchanged over the 170 Myr from $z \sim 8$ to $z \sim 10$. This implies that the wide area data provides essentially 30% of the total search power in case of an LF evolution in ϕ_* only.

Given that we only detect one probable candidate, the LF appears to drop faster than expected from the empirical lower redshift extrapolation. In particular, we do not detect the ~ 6 galaxies that we would have expected to find at $z \sim 10$ if the lower redshift trends remained valid. From these extrapolations we predicted to find three sources in the HUDF (consistent with the expectations from Bouwens et al. 2011a) and about one in each of the two HUDF09 parallel fields.

The Poissonian probability to find ≤ 1 source, given that 6 are expected is $< 2\%$. This remains significant, even after including cosmic variance, which adds an additional uncertainty on these low number counts of about 45 – 50% for an individual WFC3/IR pointing (see e.g., Trenti & Stiavelli 2008; Robertson 2010). We derive an upper limit of 6% to the probability of finding ≤ 1 source in our search area, based on the cosmic variance calculator of Trenti & Stiavelli (2008) and combining the number counts uncertainty in the different fields assuming the final distribution is Gaussian (justified by the central limit theorem). Therefore, the detection of an accelerated evolution relative to the low-redshift extrapolation is significant at $\geq 94\%$.

4.3. Constraints on the $z \sim 10$ Luminosity Function

The accelerated evolution in the UV LF can also be seen from our constraints on the $z \sim 10$ LF. The step-wise LF is computed using an approximation of the effective selection volume as a function of observed magnitude $V_{\text{eff}}(m) = \int_0^\infty dz \frac{dV}{dz} S(z, m) C(m)$. The LF in bins of absolute magnitude is then given by $\phi(M_i) dM = N_i^{\text{obs}} / V_{\text{eff}}(m_i)$. This is shown in Figure 7, where the LF was evaluated in bins of 0.5 mag, and non-detections correspond to 1σ upper limits including the effects of 50% cosmic variance per pointing.

As can be seen in Figure 7, the current constraints on the $z \sim 10$ LF are significant even at bright magnitudes where the wide area data are particularly valuable. These data sets reduce the upper limits by more than an order of magnitude relative to using only the HUDF09 fields, therefore indicating that the $z \sim 10$ LF at $M_{1400} < -20$ drops by a factor $\sim 4 - 5$ with respect to the observed LF at $z \sim 8$. However, from these shallow data sets, no constraints can be obtained on any accelerated evolution of the UV LF around $z \sim 8 - 10$. This only becomes apparent at $M_{1400} > -20$ (corresponding to $H_{160, AB} \sim 27.5$ mag). Such faint limits are only probed by the HUDF09 data set. In particular, at $M_{1400} = -19$, the upper limit on the LF is a factor ~ 3 below the expectation (Fig. 7). Thus, it is clear that data reaching to deeper than $H_{160, AB} = 28.5$ mag will be necessary to further constrain the drop in the LF in the future (which is beyond the reach of the current MCT programs).

In order to quantify the change in the LF from $z \sim 10$ to $z \sim 8$ more robustly, we consider two possible scenarios. First, we assume the accelerated LF evolution occurs only in M_* , at a constant rate since $z \sim 6$, and we fit the

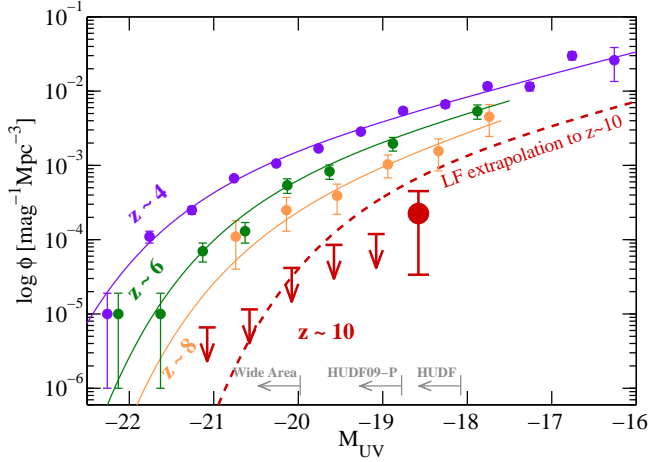


FIG. 7.— Constraints on the $z \sim 10$ LF from our combined data set, evaluated in 0.5 mag bins. The upper limits correspond to 1σ Poissonian limits including the additional uncertainty of 50% cosmic variance per pointing. It is clear that the luminosity function evolves strongly from $z \sim 8$ to $z \sim 10$, as our upper limits are a factor ~ 2 -5 below the measured $z \sim 8$ LF of Bouwens et al. (orange data; 2011b). The expected $z \sim 10$ LF as extrapolated from fits to lower redshift LBG LFs is shown as a dashed red line. Using this LF, we would expect to detect six sources in the full data set (~ 3.4 in the HUDF, and ~ 1.2 in each of the HUDF09 parallels; see Figure 6). For comparison also the $z \sim 4$ and $z \sim 6$ LFs are plotted (Bouwens et al. 2007), showing the dramatic build-up of UV luminosity across ~ 1 Gyr of cosmic time. The light gray vectors along the lower axis indicate the range of luminosities over which the different data sets dominate the $z \sim 10$ LF constraints.

Poissonian likelihood for the observed number of sources. This can be written as $\mathcal{L} = \prod_j \prod_i P(N_{j,i}^{\text{obs}}, N_{j,i}^{\text{exp}})$, where j runs over all fields, and i runs over the different magnitude bins, and P is the poissonian probability.

Our extrapolation of the UV LF is a modification of the fitting formulae of Bouwens et al. (2011b). We thus use $\phi_*(z) = 1.14 \times 10^{-3} \text{ Mpc}^{-3} = \text{const.}$ and $\alpha(z) = -1.73 = \text{const.}$, and assume: $M_*(z) = -20.29 + \zeta(z-6)$. We then fit for ζ , finding $\zeta = 0.58^{+0.14}_{-0.11}$, which results in an estimate for $M_*(z=10) = -18.0 \pm 0.5 \text{ mag.}$

Alternatively, we assume $M_*(z) = -19.63 = \text{const.}$ (as derived for $z \sim 8$ from our empirical extrapolation), $\alpha = -1.73$, and we fit only for an evolution in the normalization with redshift relative to the $z \sim 8$ LF. This results in $\phi_* = 1.14 \times 10^{-3} 10^{-\Upsilon(z-8)} \text{ Mpc}^{-3}$, with best fit $\Upsilon = 0.54^{+0.36}_{-0.19}$. Thus, using this extrapolation, the normalization of the UV LF from $z \sim 10$ to $z \sim 8$ is expected to increase by a factor 12. These results are summarized in Table 3.

4.4. Evolution in Luminosity Density From $z \sim 10$ to $z \sim 8$

The quantity most easily comparable between observations and simulations is the observed luminosity density (ρ_L) above a given limiting magnitude, which is shown in Figure 8. The LD from the $z \sim 10$ candidate alone amounts to $\log_{10} \rho_L = 24.1^{+0.5}_{-0.7} \text{ erg s}^{-1} \text{ Hz}^{-1} \text{ Mpc}^{-3}$. However, a more realistic estimate of the luminosity density can be obtained from the two possible extrapolations of the UV LF we derived in the previous section, which include the contribution from galaxies at $M_{1400} < -19 \text{ mag}$ that are currently undetected. Assuming the LF evolution only occurs in the characteris-

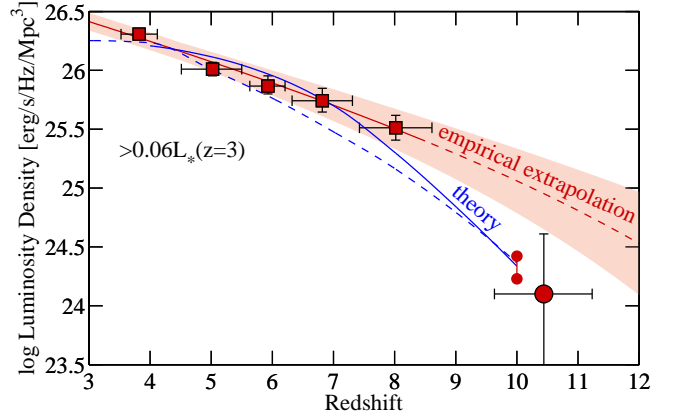


FIG. 8.— The evolution of the UV luminosity density ρ_L above $M_{1400} = -18 \text{ mag}$ ($> 0.06 L_*$ at $z=3$). The filled circle at $z \sim 10.4$ is the luminosity density directly measured for our only $z \sim 10$ galaxy candidate. The two connected dots at $z = 10$ show the range of possible LD values, given the two simple, accelerated extrapolations of the UV luminosity function described in section 4.3. The red line corresponds to the empirical LF evolution from Bouwens et al. (2011b). Its extrapolation to $z > 8$ is shown as dashed red line. The ρ_L data at $z \sim 4 - 8$ is taken from Bouwens et al. (2007); Bouwens et al. (2011b). As can be seen, ρ_L increases by more than an order of magnitude in the 170 Myr from $z \sim 10$ to $z \sim 8$, indicating that the galaxy population at this luminosity range evolves by a factor ≥ 4 more than expected from low redshift extrapolations. The predicted ρ_L evolution of the semi-analytical model of Lacey et al. (2011) is shown as dashed blue line, and the theoretical model prediction of Trenti et al. (2010) is shown as blue solid line. These reproduce the expected luminosity density at $z \sim 10$ remarkably well.

tic luminosity, we find for the $z \sim 10$ luminosity density $\log_{10} \rho_L = 24.2 \pm 0.5 \text{ erg s}^{-1} \text{ Hz}^{-1} \text{ Mpc}^{-3}$, while assuming the evolution to be driven by a normalization of the Schechter function only, we find $\log_{10} \rho_L = 24.4 \pm 0.5 \text{ erg s}^{-1} \text{ Hz}^{-1} \text{ Mpc}^{-3}$. These different estimates are also summarized in Table 3.

Given that the observed luminosity density at $z \sim 8$ is $\log_{10} \rho_L(z=8) = 25.6 \text{ erg s}^{-1} \text{ Hz}^{-1} \text{ Mpc}^{-3}$ (Bouwens et al. 2011b), the inferred increase in luminosity density in the 170 Myr from $z \sim 10$ to $z \sim 8$ amounts to more than an order of magnitude. This is a factor ≥ 4 higher than what would have been inferred from the empirical relation for the UV LF evolution, which predicts an increase by only a factor ~ 3 .

Note however, that such a rapid increase in luminosity density is actually predicted by many theoretical models. In Figure 8 we also show the luminosity densities at $M_{1400} < -18 \text{ mag}$ as derived from the semi-analytical model (SAM) of Lacey et al. (2011), and from the theoretical model of Trenti et al. (2010).

Although there is still some discrepancy on the exact shape of the $z > 6$ UV LF between the Lacey et al. (2011) SAM and the observations, the integrated luminosity density and its evolution is remarkably well reproduced across the full redshift range $z \sim 4 - 8$ (see also discussion in Raićević et al. 2011). The semi-analytic model predicts a constant growth in ρ_L with cosmic time at somewhat faster pace than observed, leading to some discrepancy between the observations and the model at $z \sim 7$ and $z \sim 8$, where the observational data shows higher luminosity densities. However, the model reproduces our estimates of the $z \sim 10$ LD remarkably well.

Similar conclusions are reached for the purely the-

TABLE 3
SUMMARY OF $z \sim 10$ LF AND LUMINOSITY DENSITY ESTIMATES

$\log_{10} \phi_*(z=10)$ [$\text{Mpc}^{-3}\text{mag}^{-1}$]	$M_*(z=10)$	α	$\log_{10} \rho_L^\dagger$ [$\text{erg s}^{-1}\text{Hz}^{-1}\text{Mpc}^{-3}$]	$\log_{10} \rho_*$ [$M_\odot\text{yr}^{-1}\text{Mpc}^{-3}$]
-2.9 (fixed)	-18.0 ± 0.5	-1.73 (fixed)	24.2 ± 0.5	-3.7 ± 0.5
-4.0 ± 0.5	-19.63 (fixed)	-1.73 (fixed)	24.4 ± 0.5	-3.5 ± 0.5
	single candidate		$24.1^{+0.5}_{-0.7}$	$-3.8^{+0.5}_{-0.7}$

† Integrated down to $0.06L_{z=3}^*$ ($M_{1400} = -18$ mag)

oretical model of Trenti et al. (2010). In particular, this model predicts the UV LD to evolve at an accelerated rate at $z > 8$, being only $\log_{10} \rho_L = 24.4 \text{ erg s}^{-1}\text{Hz}^{-1}\text{Mpc}^{-3}$ at $z \sim 10$, in excellent agreement with our observed estimates. Since the model is only based on the evolution of the underlying dark matter mass function, this indicates that an accelerated evolution in the galaxy population can be explained even without the need for a change in the physical mechanisms of galaxy formation.

For further theoretical model predictions, see also e.g. Mao et al. (2007); Salvaterra et al. (2011), or Muñoz (2011).

It is also interesting to note that the star-formation rate densities (see Table 3) inferred from our data, are more than an order of magnitude too low to account for the stellar mass densities observed at $z \sim 7$ in systems of similar brightness. With constant star-formation over ~ 300 Myr from $z \sim 10$ to $z \sim 7$ the observed galaxy population would only produce a stellar mass density of $\log_{10} \rho_M = 4.7 - 5.3 M_\odot \text{Mpc}^{-3}$, compared to $\log_{10} \rho_M(z=7) = 6.6 M_\odot \text{Mpc}^{-3}$ as estimated by, e.g., Labbé et al. (2010b,a); Gonzalez et al. (2010). If the inferred mass densities and SFRs are correct, this suggests that the majority of the stars found in $z \sim 7$ galaxies down to $M_{UV} < -18$ mag have to be formed in systems below our detection limit at $z \sim 10$ or are younger than 300 Myr.

5. SUMMARY AND CONCLUSIONS

In this paper, we have extended our search for $z \sim 10$ galaxies to $\sim 160 \text{ arcmin}^2$ of public WFC3/IR data obtained around the GOODS South field (see Figure 1). These data sets have been acquired through the three surveys HUDF09, ERS, and CANDELS, and reach to varying depths, from $H_{160,AB} = 26.9$ to $H_{160,AB} = 29.4$. Based on strict optical non-detection requirements and a color cut of $J_{125} - H_{160} > 1.2$, we search these fields for Lyman Break J_{125} -dropout galaxies, which are expected to lie at $z > 9.5$. A total of 17 sources satisfy these criteria. However, 16 out of these sources show strong IRAC detections which rule out their being at such very high redshifts. Rather, these galaxies are found to have best-fit photometric redshifts in the range $z_{phot} = 2 - 4$ (see section 3.4 and appendix). They remain undetected in the optical due to their evolved stellar populations with non-negligible dust obscuration. This shows how important Spitzer IRAC data is for removing contaminating lower redshift galaxies.

Interestingly, these contaminants are essentially only detected with magnitudes in the range $H_{160,AB} = 24 - 26$ mag. This is ~ 1 mag brighter than the detection limits of our bright surveys, which suggests that such evolved

and dusty galaxies follow a peaked luminosity function at these wavelengths. If confirmed by future wide-area WFC3/IR data sets, this would indicate that such extremely red systems are not as much of a problem for $z > 9$ searches at fainter levels as has been expected to date. However, the existence of such galaxy populations will make it challenging to use large-area WFC3 surveys such as pure-parallel fields (e.g. Trenti et al. 2011) for constraining the bright end of the $z \sim 10$ UV LF without additional follow-up observations to validate the candidates.

Even with our expanded search area, the only $> 5\sigma$ detected galaxy with a color limit of $H_{160} - [3.6] < 1.6$ (2σ) and thus the only possible $z \sim 10$ galaxy candidate is the same source that we reported already in Bouwens et al. (2011a). In appendix B we additionally note one other lower S/N candidate that is suggestive of being at comparable redshift, but requires confirmation from further HST WFC3/IR data.

Interestingly, we would have expected to detect six $z \sim 10$ galaxies in our data, if the UV LF evolved to $z \sim 10$ as expected from lower redshift trends (see §4.2). Thus, the galaxy population appears to evolve at an accelerated rate beyond $z > 8$. We infer that the UV luminosity density increases by more than an order of magnitude in only 170 Myr from $z \sim 10$ to $z \sim 8$, and we are thus likely witnessing the first massive build-up of the galaxy population at these early epochs in the reionization era. The fact that theoretical models based on the evolution of dark matter halos do, in fact, predict such an accelerated increase in the LD, indicates that these rapid changes are mainly driven by an accelerated evolution of the underlying dark matter mass function, rather than due to a change in star-formation properties of these early galaxies (see e.g., Trenti et al. 2010; Lacey et al. 2011).

The accelerated evolution of the galaxy population also has interesting consequences for cosmic reionization by galaxies brighter than $M_{UV} = -18$ mag, the current detection limits. With such a sharp decrease in the luminosity density above $z \sim 8$, it is impossible for such bright galaxies alone to create a reionization history in agreement with the high optical depth measurement of WMAP and the vast majority of the ionizing flux has to be created by fainter galaxies (see also Bouwens et al. 2011c).

Unfortunately, our knowledge of galaxies at $z > 8$ still remains very uncertain. However, WFC3/IR offers unique opportunities to make significant progress in expanding the number of galaxies at $z \sim 9 - 10$ and addressing some of the key issues related to early galaxy formation and its impact on reionization, even before the advent of JWST. In Figure 9, we show the depth re-

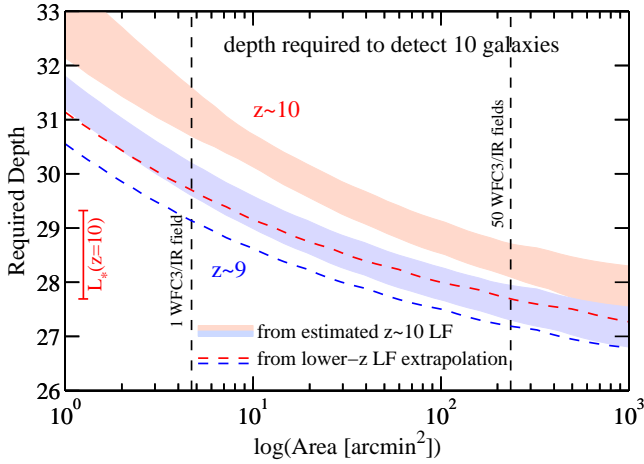


FIG. 9.— Depth required to detect ten $z \sim 9$ galaxies (blue shaded region and dashed line) and ten $z \sim 10$ galaxies (red shaded region and dashed line) as a function of survey area. These regions show the expected number of sources calculated using our LF extrapolations to $z \sim 10$ from section 4.3, i.e. assuming only evolution in M_* or only in ϕ_* to reproduce the detection of our one $z \sim 10$ candidate. The dashed lines show the same, but assuming the standard lower-redshift extrapolation of the UV LF (Bouwens et al. 2011b). In particular, at $z \sim 10$ the estimated depths differ significantly. The range of $L_*(z = 10)$ values of these extrapolations is indicated with an errorbar in the lower left. As can be seen, surveys reaching significantly deeper than ~ 28 mag will be required to detect a significant population of $z > 8$ galaxies. The vertical dashed lines indicate the area of one and 50 WFC3/IR fields, respectively. A survey with only one pointing would need to reach to ~ 31 mag in $H_{160,AB}$ to significantly constrain the $z \sim 10$ galaxy population, which is out of reach with HST WFC3/IR. Therefore, multiple fields are favorable for searching for $z \sim 10$ galaxies. Additionally, comparably deep optical data (> 30 mag) and deep IRAC imaging would be required over such fields in order to robustly exclude low-redshift contaminants. The identification of $z \sim 9$ galaxies would benefit from imaging in different filters (e.g., F140W) than adopted in current deep WFC3/IR fields.

quired to detect ten $z \sim 9$ and ten $z \sim 10$ galaxies for a given survey area. Such future data sets will have to reach significantly fainter than ~ 28 mag to accomplish this goal, even for large surveyed areas of 50 WFC3/IR fields. This is deeper than currently planned wide-area WFC3/IR data (including MCT programs). In fact, to characterize the luminosity function at luminosities below L_* and to set better constraints for reionization, surveys to fainter than 29 AB mag are really needed. Note that with only one WFC3/IR field, a magnitude of ~ 31 has to be reached to detect a significant $z \sim 10$ population, which is fainter than is practical with HST.

Based on the current LF constraints, we find that imaging a few fields provides the best chance to improve on current $z \sim 10$ constraints. Furthermore, in order to further constrain the possible accelerated evolution of the UV LF, the $z \sim 9$ regime offers the best opportunity. A sizable population of $z \sim 9$ galaxies is expected to be seen already down to ~ 29 mag over multiple WFC3/IR fields, which can be achieved with the efficient F140W filter. Thus, it is likely that already with WFC3/IR, we can soon push the frontier of statistical galaxy samples with WFC3/IR from $z \sim 8$ another $\sim 100 - 170$ Myr back out to $z \sim 9 - 10$.

Support for this work was provided by NASA through Hubble Fellowship grant HF-51278.01 awarded by the Space Telescope Science Institute, which is operated by the Association of Universities for Research in Astronomy, Inc., for NASA, under contract NAS 5- 26555. This work has been supported by NASA grant NAG5-7697 and NASA grant HST-GO-11563.01.

Facilities: HST(ACS/WFC3), Spitzer(IRAC).

REFERENCES

- Beckwith, S. V. W., et al. 2006, *AJ*, 132, 1729
 Bertin, E., & Arnouts, S. 1996, *A&AS*, 117, 393
 Bouwens, R., Broadhurst, T., & Illingworth, G. 2003, *ApJ*, 593, 640
 Bouwens, R. J., Illingworth, G. D., Blakeslee, J. P., Broadhurst, T. J., & Franx, M. 2004, *ApJ*, 611, L1
 Bouwens, R. J., Illingworth, G. D., Franx, M., & Ford, H. 2007, *ApJ*, 670, 928
 Bouwens, R. J., Illingworth, G. D., Thompson, R. I., & Franx, M. 2005, *ApJ*, 624, L5
 Bouwens, R. J., et al. 2009, *ApJ*, 705, 936
 —. 2010a, *ApJ*, 709, L133
 —. 2010b, *ApJ*, 708, L69
 —. 2011a, *Nature*, 469, 504
 —. 2011b, *ApJ*, 737, 90
 —. 2011c, *ArXiv e-prints*, 1105.2038
 Bruzual, G., & Charlot, S. 2003, *MNRAS*, 344, 1000
 Bunker, A., et al. 2010, *MNRAS*, 409, 855
 Calzetti, D., Armus, L., Bohlin, R. C., Kinney, A. L., Koornneef, J., & Storchi-Bergmann, T. 2000, *ApJ*, 533, 682
 Coleman, G. D., Wu, C., & Weedman, D. W. 1980, *ApJS*, 43, 393
 Damen, M., Labbé, I., Franx, M., van Dokkum, P. G., Taylor, E. N., & Gawiser, E. J. 2009, *ApJ*, 690, 937
 Dickinson, M., Giavalisco, M., & GOODS Team. 2003, in *The Mass of Galaxies at Low and High Redshift*, ed. R. Bender & A. Renzini, 324+
 Dunlop, J. S., McLure, R. J., Robertson, B. E., Ellis, R. S., Stark, D. P., Cirasuolo, M., & de Ravel, L. 2011, *ArXiv e-prints*, 1102.5005
 Feldmann, R., et al. 2006, *MNRAS*, 372, 565
 Ferguson, H. C., et al. 2004, *ApJ*, 600, L107
 Finkelstein, S. L., Papovich, C., Giavalisco, M., Reddy, N. A., Ferguson, H. C., Koekemoer, A. M., & Dickinson, M. 2010, *ApJ*, 719, 1250
 Giavalisco, M., et al. 2004, *ApJ*, 600, L93
 Gonzalez, V., Labbe, I., Bouwens, R., Illingworth, G., Franx, M., & Kriek, M. 2010, *ArXiv e-prints*, 1008.3901
 Grazian, A., et al. 2010, *ArXiv e-prints*, 1011.6569
 Grogin, N. A., et al. 2011, *ArXiv e-prints*, 1105.3753
 Henry, A. L., Malkan, M. A., Colbert, J. W., Siana, B., Teplitz, H. I., & McCarthy, P. 2008, *ApJ*, 680, L97
 Henry, A. L., et al. 2009, *ApJ*, 697, 1128
 Iwata, I., Ohta, K., Tamura, N., Akiyama, M., Aoki, K., Ando, M., Kiuchi, G., & Sawicki, M. 2007, *MNRAS*, 376, 1557
 Koekemoer, A. M., et al. 2004, *ApJ*, 600, L123
 Koekemoer, A. M., et al. 2011, *ArXiv e-prints*, 1105.3754
 Komatsu, E., et al. 2011, *ApJS*, 192, 18
 Labbé, I., et al. 2010a, *ApJ*, 716, L103
 —. 2010b, *ApJ*, 708, L26
 Lacey, C. G., Baugh, C. M., Frenk, C. S., & Benson, A. J. 2011, *MNRAS*, 45
 Lorenzoni, S., Bunker, A. J., Wilkins, S. M., Stanway, E. R., Jarvis, M. J., & Caruana, J. 2011, *MNRAS*, 414, 1455
 Mao, J., Lapi, A., Granato, G. L., de Zotti, G., & Danese, L. 2007, *ApJ*, 667, 655
 McLure, R. J., Cirasuolo, M., Dunlop, J. S., Foucaud, S., & Almaini, O. 2009, *MNRAS*, 395, 2196
 McLure, R. J., Dunlop, J. S., Cirasuolo, M., Koekemoer, A. M., Sabbie, E., Stark, D. P., Targett, T. A., & Ellis, R. S. 2010, *MNRAS*, 403, 960
 Mobasher, B., et al. 2005, *ApJ*, 635, 832
 Muñoz, J. A. 2011, *arXiv:1104.0927*
 Oesch, P. A., et al. 2007, *ApJ*, 671, 1212
 —. 2009, *ApJ*, 690, 1350
 —. 2010a, *ApJ*, 709, L21
 —. 2010b, *ApJ*, 714, L47
 —. 2010c, *ApJ*, 709, L16
 Oke, J. B., & Gunn, J. E. 1983, *ApJ*, 266, 713
 Ouchi, M., et al. 2004, *ApJ*, 611, 660
 Raičević, M., Theuns, T., & Lacey, C. 2011, *MNRAS*, 410, 775

Richard, J., Stark, D. P., Ellis, R. S., George, M. R., Egami, E., Kneib, J., & Smith, G. P. 2008, *ApJ*, 685, 705
 Robertson, B. E. 2010, *ApJ*, 713, 1266
 Rodighiero, G., Cimatti, A., Franceschini, A., Brusa, M., Fritz, J., & Bolzonella, M. 2007, *A&A*, 470, 21
 Salvaterra, R., Ferrara, A., & Dayal, P. 2011, *MNRAS*, 414, 847
 Santini, P., et al. 2009, *A&A*, 504, 751
 Sawicki, M., & Thompson, D. 2006, *ApJ*, 642, 653
 Schaerer, D., & de Barros, S. 2009, *A&A*, 502, 423
 —. 2010, *A&A*, 515, A73+
 Stanway, E. R., McMahon, R. G., & Bunker, A. J. 2005, *MNRAS*, 359, 1184
 Stark, D. P., Ellis, R. S., Richard, J., Kneib, J., Smith, G. P., & Santos, M. R. 2007, *ApJ*, 663, 10
 Stutz, A. M., Papovich, C., & Eisenstein, D. J. 2008, *ApJ*, 677, 828
 Trenti, M., & Stiavelli, M. 2008, *ApJ*, 676, 767
 Trenti, M., Stiavelli, M., Bouwens, R. J., Oesch, P., Shull, J. M., Illingworth, G. D., Bradley, L. D., & Carollo, C. M. 2010, *ApJ*, 714, L202

Trenti, M., et al. 2011, *ApJ*, 727, L39+
 Wiklind, T., Dickinson, M., Ferguson, H. C., Giavalisco, M., Mobasher, B., Grogin, N. A., & Panagia, N. 2008, *ApJ*, 676, 781
 Wilkins, S. M., Bunker, A. J., Ellis, R. S., Stark, D., Stanway, E. R., Chiu, K., Lorenzoni, S., & Jarvis, M. J. 2010, *MNRAS*, 403, 938
 Wilkins, S. M., Bunker, A. J., Lorenzoni, S., & Caruana, J. 2011, *MNRAS*, 411, 23
 Wilkins, S. M., Bunker, A. J., Stanway, E., Lorenzoni, S., & Caruana, J. 2011, arXiv:1106.5977
 Windhorst, R. A., et al. 2011, *ApJS*, 193, 27
 Yan, H., Windhorst, R. A., Hathi, N. P., Cohen, S. H., Ryan, R. E., O’Connell, R. W., & McCarthy, P. J. 2010, *Research in Astronomy and Astrophysics*, 10, 867

APPENDIX

A. THE INTERMEDIATE REDSHIFT CONTAMINANTS

Here we briefly summarize the properties of the galaxies that formally met the J_{125} -dropout criteria based on the HST data alone, but which were found to exhibit very red H_{160} to IRAC colors. This makes it extremely unlikely that these galaxies are at $z \gtrsim 9$. A summary of these sources is listed in Table 4.

Note that all these galaxies are obviously clearly detected in the IRAC images, with the exception of one source (jD-2080646581), which is close to a quintet of IRAC bright galaxies. However, after subtraction of the contaminating flux from its neighbors based on a careful convolution of the H_{160} image to the IRAC PSFs (see, e.g., Labbé et al. 2010b,a; Gonzalez et al. 2010) it also shows a clear detection (see Fig. 11). The best estimate for its color is $H_{160} - [3.6] = 1.6 \pm 0.5$, which is too red for a likely $z > 9$ source.

Interestingly, six of these 16 sources are present in catalogs of potential passive high redshift galaxies of Rodighiero et al. (2007) and Wiklind et al. (2008). One of these is also detected in X-ray emission and classified as a so-called EXO source hosting a potentially highly obscured AGN, particularly if it is an evolved galaxy at intermediate redshift, as pointed out by Koekemoer et al. (2004).

We have derived photometric redshifts and mass estimates for these galaxies by complementing our HST photometry with the IRAC fluxes from the GOODS MUSIC catalog (Santini et al. 2009) or from the SIMPLE images. Based on SED fits with Bruzual & Charlot (2003) models, these galaxies are confirmed to be evolved, reddened systems with stellar masses around $10^{11} M_{\odot}$ at redshifts $z \sim 2 - 3.5$. Note that with the exception of four sources these are all detected individually in MIPS $24\mu\text{m}$ data.

In Figure 10 we additionally show the surface density of these evolved intermediate redshift sources. Even at their peak surface density, they are only found at 0.06 sources per magnitude per arcmin². Therefore, only ~ 0.4 sources are expected per WFC3/IR pointing, providing an explanation for why none of these bright sources are found in the three deep HUDF09 fields. The dearth of such galaxies faintward of $H_{160,AB} = 26$, at ~ 1 mag brighter than the completeness limit of our bright surveys, suggests that such extremely red sources become even less frequent (i.e., that their LF may have peaked at these magnitudes) and so they could be less problematic for contamination of fainter

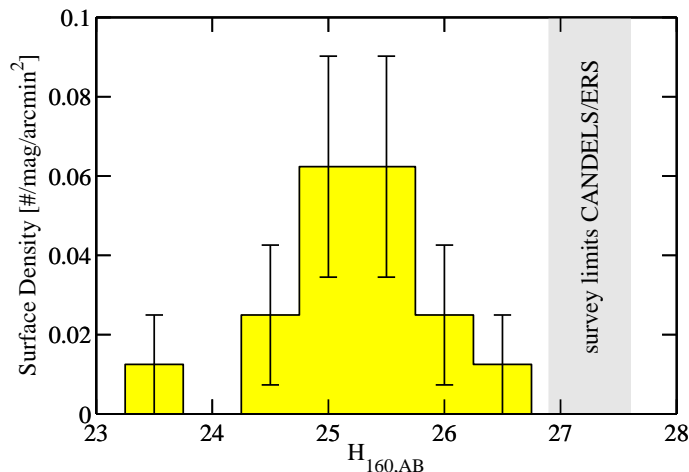


FIG. 10.— The surface density of contaminating sources at redshifts $z \sim 2 - 4$. The surface densities are extremely low. Only ~ 0.4 sources are expected per WFC3/IR pointing. The rapid disappearance of such sources beyond $H_{160,AB} \gtrsim 26$, almost one mag brighter than the detection limits of our shallow fields from ERS and CANDELS, suggests that such sources may have a peaked LF at the wavelengths of interest in these surveys and so could be less of a problem for contamination for fainter $z \sim 10$ galaxy samples.

TABLE 4
LOWER REDSHIFT CONTAMINANTS THAT SATISFY THE J-DROPOUT CRITERIA, BUT SHOW STRONG IRAC DETECTIONS.

ID	α	δ	H_{160}	$J_{125} - H_{160}$	S/N_{H160}	$r_{1/2}['']$	MUSIC-ID [†]	references
<i>ERS</i>								
jD-2162843432	03:32:16.28	-27:43:43.2	23.6 ± 0.1	1.32 ± 0.11	14.6	0.65	70081	—
jD-2188742241	03:32:18.87	-27:42:24.1	25.5 ± 0.1	1.36 ± 0.23	12.2	0.29	70040	—
jD-2226644214	03:32:22.66	-27:44:21.4	25.5 ± 0.1	1.80 ± 0.38	10.9	0.26	70104	—
<i>CANDELS-Deep</i>								
jD-2487849357	03:32:48.78	-27:49:35.7	25.2 ± 0.1	1.36 ± 0.25	11.4	0.33	70314	—
jD-2532547516	03:32:53.25	-27:47:51.6	25.3 ± 0.2	1.55 ± 0.32	11.2	0.26	70236	4
jD-2304648166	03:32:30.46	-27:48:16.6	24.8 ± 0.1	1.23 ± 0.11	29.4	0.23	70258	1
jD-2387448399	03:32:38.74	-27:48:39.9	24.9 ± 0.1	1.41 ± 0.22	14.9	0.33	70273	1,2,4
jD-2412344008	03:32:41.23	-27:44:00.8	25.8 ± 0.2	1.43 ± 0.30	11.0	0.22	70092	—
jD-2158349541	03:32:15.83	-27:49:54.1	24.4 ± 0.1	1.60 ± 0.15	19.1	0.38	70316	1
jD-2249748085	03:32:24.97	-27:48:08.5	25.7 ± 0.2	1.61 ± 0.43	7.5	0.33	70252	—
jD-2080646581	03:32:08.06	-27:46:58.1	26.5 ± 0.3	2.01 ± 0.67	6.1	0.16	—	—
<i>CANDELS-Wide</i>								
jD-2489152264	03:32:48.91	-27:52:26.4	25.2 ± 0.1	1.49 ± 0.27	12.3	0.26	70442	—
jD-2358952367	03:32:35.89	-27:52:36.7	25.1 ± 0.2	2.27 ± 0.94	7.2	0.35	70455	1
jD-2351353198	03:32:35.13	-27:53:19.8	25.4 ± 0.2	1.61 ± 0.43	5.8	0.35	70484	—
jD-2331152057	03:32:33.11	-27:52:05.7	26.2 ± 0.3	1.24 ± 0.54	5.8	0.20	70429	1,3
jD-2211356269	03:32:21.13	-27:56:26.9	24.4 ± 0.1	1.47 ± 0.22	7.9	0.44	—	—

REFERENCES. — (1) Rodighiero et al. (2007); (2) Mobasher et al. (2005); (3) Koekemoer et al. (2004); (4) Wiklind et al. (2008)

[†] From Santini et al. (2009).

$z \gtrsim 9$ dropout searches. This will have to be confirmed, however, with future wide-area WFC3/IR data, searching explicitly for this type of galaxies.

Note that our finding of a disappearance of passive intermediate redshift galaxies to fainter magnitudes is in agreement with Stutz et al. (2008), who found an absence of passive, red galaxies at $z \sim 1.5 - 3$ at masses below $\sim 10^{10} M_{\odot}$.

B. POTENTIAL FUTURE EXTENSION OF THE HUDF $Z \sim 10$ CANDIDATE SAMPLE

As pointed out in section 5, due to the apparent paucity of such sources, it will be difficult to extend the $z \sim 10$ candidate lists to large numbers of reliable sources in the near future with HST. In cycle 18, an additional 128 orbit imaging survey was granted (PI: Ellis) to further study the $z \gtrsim 7$ galaxy population over the HUDF data. However, given that only one single field will be targeted and that only a relatively small amount of H_{160} data is currently planned to be taken (22 new orbits, relative to the ~ 58 already available from the HUDF09 and CANDELS programs), we can forecast what this program will bring in terms of $z \sim 10$ galaxy science. Essentially, every 5σ source that will be obtained as a result of this new program should already be present as a 4.2σ source in the current H_{160} band data. We therefore systematically searched for lower significance sources (down to 4σ detections) that satisfy our $z \sim 10$ dropout criteria. Essentially, the only additional candidate that we found is already detected at 4.8σ in the current data, and is located at RA=03:32:43.01, DEC=-27:46:53.3 (see also Yan et al. 2010). Note, however, that the i_{775} -band data shows very faint positive flux ($\sim 1.5\sigma$) exactly at the location of this source, which increases the chance that it is at lower redshift. This demonstrates the value of even deeper optical data over these fields for more robust high redshift galaxy selections. Given the scarcity of low significance candidates in the HUDF, it is clear, however, that it will be very important to image at least one additional field to similar depth in order to further constrain the accelerated evolution in the cosmic star-formation rate density (see Fig. 9).

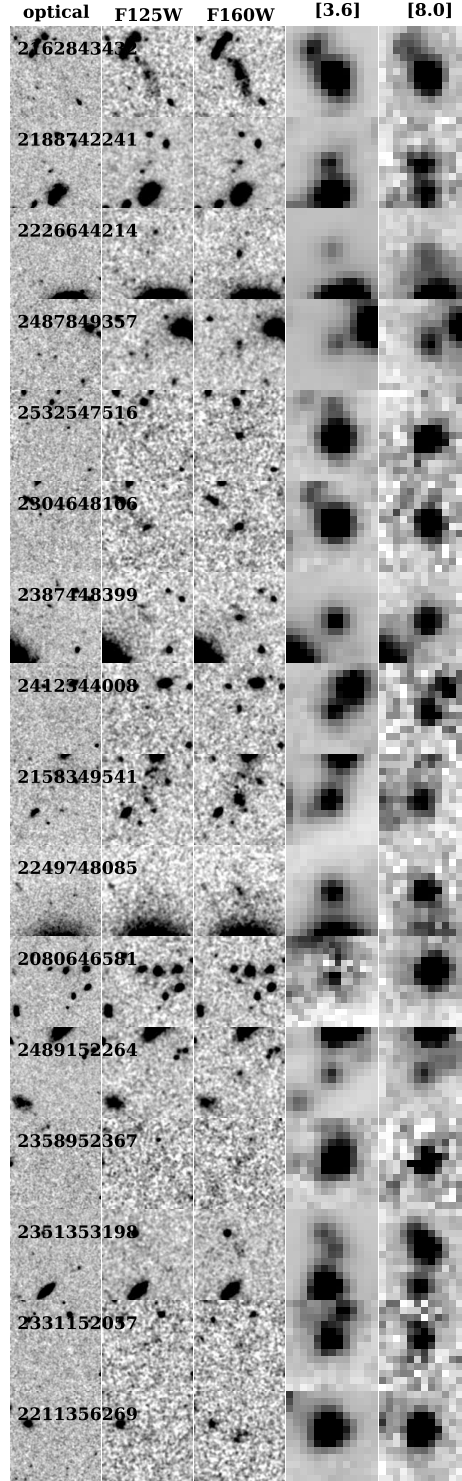


FIG. 11.— Images of all optical undetected sources with $J_{125} - H_{160} > 1.2$ mag, but with strong IRAC detections. This rules out the possibility that these sources are at $z > 9$. The images are 7.5 arcsec on a side, and show from left to right (1) a stack of B_{435} , V_{606} , i_{775} , z_{850} , (2) J_{125} , (3) H_{160} , (4) Spitzer IRAC [3.6], and (5) IRAC [8.0]. All these sources are clearly detected in all IRAC bands, including [8.0]. Thus, their $H_{160} - [8.0]$ colors are greater than ~ 2 , which is very different from the relatively flat color expected for a real $z \sim 10$ source. Note that IRAC flux of the source jD-2080646581 is heavily contaminated by neighboring sources. In the [3.6] band, we therefore show the cleaned image, after subtraction of the contaminating flux, which reveals its clear detection.